PHYSICAL REVIEW D VOLUME 25, NUMBER 5 1 MARCH 1982

Tests of low-energy parity restoration at e^+e^- and ep colliders

Thomas G. Rizzo
Department of Physics and Ames Laboratory, Iowa State University, Ames, Iowa 50011
(Received 14 September 1981)

We have recently shown that the embedding of $SU(2)_L \otimes SU(2)_R \otimes U(1)_{B-L}$ into an SO(10) grand unified theory can lead to low-energy parity restoration providing an alternative to the conventional SU(5) theory (with a desert above M_W). In this paper we examine various tests of this model which can be employed at future (and present) e^+e^- and ep colliders to distinguish our model from the standard electroweak $SU(2)_L \otimes U(1)$ model.

I. INTRODUCTION

In a recent series of papers,[1] Senjanović and myself have considered the possibility of low-energy parity restoration through the embedding of the $SU(2)_L \otimes SU(2)_R \otimes U(1)_{B-L}$ electroweak gauge group into grand unified SO(10). The breaking scheme goes as follows:

$$SO(10) \underset{M_X}{\rightarrow} SU(2)_L \otimes SU(2)_R \otimes SU(4)_C \underset{M_C}{\rightarrow} SU(2)_L \otimes SU(2)_R \otimes U(1)_{B-L} \otimes SU(3)_C$$

$$\underset{M_R}{\rightarrow} SU(2)_L \otimes U(1)_Y \otimes SU(3)_C \underset{M_W}{\rightarrow} SU(3)_C \otimes U(1)_{\mathrm{QED}}$$

with $M_X \simeq 10^{15}-10^{17}$ GeV (depending on the exact Higgs structure), $M_C \simeq 10^{11}$ GeV, and $M_R \simeq$ a few times M_W (80 GeV). Such a picture has been shown to be consistent with all low-Q^2 (i.e., $Q^2 << $ gauge-boson masses squared) tests in both the neutral- and charged-current sectors as well as the constraints imposed by grand unification on the values of $\sin^2\theta_W$ and α_s. Unlike the standard SU(5) scheme[2] which demands a "desert" between M_W and M_X our scheme has two oases, one associated with the breaking of left-right symmetry at M_R, the other with quark-lepton unification at M_C. In this paper we will examine some of the consequences of the former (low M_R) for present and future e^+e^- and ep colliders.

The basic formalism for this work can be found in the earlier work of the present author[3] which will be expanded on here for our present purposes. We will find that distinguishing our scheme from the standard model will be quite impossible at either PEP or PETRA *(unless* the helicity of the final-state leptons can be measured) and will require LEP or the SLAC collider in the e^+e^- channel and TRISTAN, HERA, CHEER, or ISABELLE (with an ep option) in the ep channel since high Q^2 is needed.

Section II will contain an analysis of various comparisons of the standard $SU(2)_L \otimes U(1)_Y$ model with our left-right-symmetric model $SU(2)_L \times SU(2)_R \otimes U(1)_{B-L}$ for e^+e^- interactions from very low energies ($\sqrt{s} \simeq$ a few GeV) to the highest possible LEP energies ($\sqrt{s} \sim 250$ GeV). Similarly, Sec. III will concentrate on an analysis of various asymmetries in ep collisions which can be used to deduce the structure of neutral currents at high Q^2 to see the differences between the standard model and the one considered here. Our results and conclusions can be found in Sec. IV.

II. e^+e^- TESTS

In this section we will consider the various effects of parity- and charge-conjugation-violating

neutral currents on the reaction $e^+e^-\to\bar{f}f$, with f being some fermion species; we will concentrate on $e^+e^-\to\mu^+\mu^-$. We will follow the analysis of our earlier work (Ref. 3) and neglect all fermion mass terms and assume unpolarized e^+ and e^- beams.

We take our effective Lagrangian to be

$$\mathcal{L}=(-e\bar{e}\gamma_\mu e+Q_f e\bar{f}\gamma_\mu f)A^\mu+\sum_i[e\gamma_\mu(v_e^i+a_e^i\gamma_5)\bar{e}+\bar{f}\gamma_\mu(v_f^i+a_f^i\gamma_5)]Z_i^\mu\ , \tag{2.1}$$

where we have assumed that there are N neutral gauge bosons; the above couplings are self-explanatory. We will assume lepton universality below in that $v_e^i=v_\mu^i$ and $a_e^i=a_\mu^i$ for all i. The differential cross section for $e^+e^-\to\bar{f}f$ can now be written as

$$\frac{d\sigma}{d\Omega}=N_C{Q_f}^2\frac{\alpha^2}{4s}[A_f(1+\cos^2\theta)+2B_f\cos\theta]\ , \tag{2.2}$$

where N_C is the number of colors of the species f and θ is the center-of-mass scattering angle. In general we find that A_f and B_f can be written as

$$A_f=1+2\sum_i\left[\frac{v_e v_f}{-Q_f e^2}\right]_i\frac{s}{(s-{M_{Z_i}}^2)}+\sum_{i,i'}\frac{(v_{e_i}v_{e_{i'}}+a_{e_i}a_{e_{i'}})(v_{f_i}v_{f_{i'}}+a_{f_i}a_{f_{i'}})}{({Q_f}^2e^4)}\frac{s}{s-{M_Z}^2}\frac{s}{s-{M_{Z_{i'}}}^2}\ , \tag{2.3}$$

$$B_f=2\sum_i\left[\frac{a_e a_f}{-Q_f e^2}\right]_i\frac{s}{s-{M_{Z_i}}^2}+\sum_{i,i'}\frac{(v_{e_i}a_{e_{i'}}+v_{e_{i'}}a_{e_i})(v_{f_i}a_{f_{i'}}+v_{f_{i'}}a_{f_i})}{({Q_f}^2e^4)}\frac{s}{s-{M_{Z_i}}^2}s-{M_{Z_{i'}}}^2\ . \tag{2.4}$$

The forward-backward charge-conjugation-violating asymmetry $A_{\rm FB}$ is then defined

$$A_{\rm FB}^f=\frac{\int_0^1 d\cos\theta\frac{d\sigma}{d\Omega}\int_{-1}^0 d\cos\theta\frac{d\sigma}{d\Omega}}{\int_{-1}^1 d\cos\theta\frac{d\sigma}{d\Omega}}=\tfrac{3}{4}B_f/A_f \tag{2.5}$$

while the total cross section is just

$$\sigma_{\rm tot}=\frac{4\pi\alpha^2}{3s}N_C{Q_f}^2A_f\ . \tag{2.6}$$

With the initial e^+,e^- beams unpolarized a net helicity in the final-state fermions result from parity-violating Z_i couplings. The differential cross section as a function of the helicity of the final fermion f can be written as

$$\left[\frac{d\sigma}{d\Omega}\right]_{h_f}=\sigma_1+h_f\sigma_2\ , \tag{2.7}$$

with

$$\sigma_1=\frac{1}{2}\frac{d\sigma}{d\Omega}\ , \tag{2.8}$$

which is given by Eq. (2.2). If we now define the helicity as

$$H^f(\theta,s)=\sigma_2/\sigma_1\ , \tag{2.9}$$

we find

$$H^f(s,\cos\theta)=\frac{-2[\Sigma_1^f(1+\cos^2\theta)+2\Sigma_2^f\cos\theta]}{A_f(1+\cos^2\theta)+2B_f\cos\theta}\ , \tag{2.10}$$

where

$$\Sigma_1^f=\sum_i\left[\frac{v_e a_f}{-Q_f e^2}\right]_i\frac{s}{(s-M_{Z_i}{}^2)}+\sum_{i,i'}\frac{(v_f a_f)_i(v_e{}^2+a_e{}^2)_{i'}}{(Q_f{}^2e^4)}\left[\frac{s}{s-M_{Z_i}{}^2}\right]\left[\frac{s}{s-M_{Z_{i'}}{}^2}\right] \tag{2.11}$$

and

$$\Sigma_2^f=\sum_i\left[\frac{v_f a_e}{-Q_f e^2}\right]_i\frac{s}{(s-M_{Z_i}{}^2)^2}+\sum_{i,i'}\frac{(v_e a_e)_i(v_f^2+a_f^2)_{i'}}{(Q_f^2e^4)}\left[\frac{s}{s-M_{Z_i}{}^2}\right]\left[\frac{s}{s-M_{Z_{i'}}{}^2}\right]. \tag{2.12}$$

The forward ($\cos\theta=1$) helicity is then

$$H_F^f=H^f(s,\cos\theta=1)=-2(\Sigma_1^f+\Sigma_2^f)/(A_f+B_f) \tag{2.13}$$

and the angular-averaged asymmetry is given by

$$\bar{H}^f=\frac{-2\int_{-1}^{1}d\cos\theta[\Sigma_1^f(1+\cos^2\theta)+2\Sigma_2^f\cos\theta]}{\int_{-1}^{1}d\cos\theta[A_f(1+\cos^2\theta)+2B_f\cos\theta]}=-2\Sigma_1^f/A_f\ . \tag{2.14}$$

In our analysis, the quantities of interest will then be A_f, $A_{\rm FB}^f$, H_F^f, and $\bar{H}^f$ specifically for $f=\mu$. For final states containing quarks with a given helicity, etc., some detailed Monte Carlo analysis is necessary before neutral-current information can be extracted from the final-state data.[4] We remind the reader that in the standard model a_f and v_f are given by

$$\begin{aligned}v_f&=e(T_3^f-2x_W Q_f)/[x_W(1-x_W)]^{1/2}\ ,\\ a_f&=eT_3^f/[x_W(1-x_W)]^{1/2}\end{aligned} \tag{2.15}$$

with $x_W=\sin^2\theta_W$ and T_3^f being the third component of weak isospin for the fermion f with charge Q_f. The above expression can be easily evaluated in the standard model as well as in the $SU(2)_2\otimes SU(2)_R\otimes U(1)_{B-L}$ model using the couplings of Ref. 1.

Let us first consider the region $\sqrt{s}\lesssim 45$ GeV/c which can be studied by PEP and PETRA and restrict ourselves to the case where the final-state fermion are muons (or τ's if universality is assumed and $m_\tau/\sqrt{s}$ neglected). The first thing we find by doing an explicit calculation is that for $\sqrt{s}\lesssim 50$ GeV a measurement of $\sigma_{\rm tot}$ will not be very valuable in distinguishing between the standard Weinberg-Salam (WS) model and left-right-symmetric (LR) model; in this energy range we find

$$\frac{\sigma_{\rm LR}-\sigma_{\rm WS}}{\sigma_{\rm LR}+\sigma_{\rm WS}}\lesssim 1.4\times10^{-3},\quad \sqrt{s}\lesssim 50\ \text{GeV}\ .$$

This is certainly much too small a fraction to be observable at any time in the forseeable future.

Next, we consider $A_{\rm FB}$ which is usually claimed as a good test of the standard model; Fig. 1 shows a comparison of the two models in the PEP/PETRA energy range. Even at the highest value of $\sqrt{s}$ the curves differ by no more than 5—10%. Clearly a measurement at the 10% level is about the best one can do at present given the low luminosity of these machines so that the present statistics cannot (or will not in the near future) be used to distinguish the two models.

Figure 2 shows the prediction of the forward and angular averaged helicities in the standard model for $\sin^2\theta_W=0.22$ and 0.23 in the energy range $\sqrt{s}\lesssim 45$ GeV. Similarly, Fig. 3 shows the

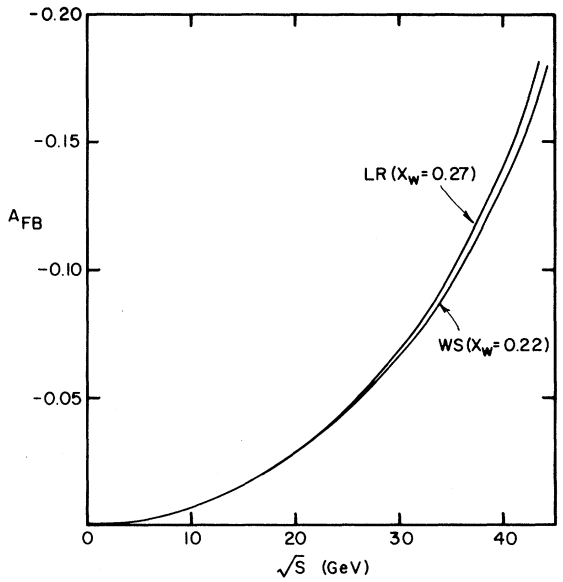

FIG. 1. The forward-backward asymmetry $A_{\rm FB}$ for the PEP/PETRA energy range for the standard model (WS) and the left-right-symmetric model (LR) in $e^+e^-\to\mu^+\mu^-$.

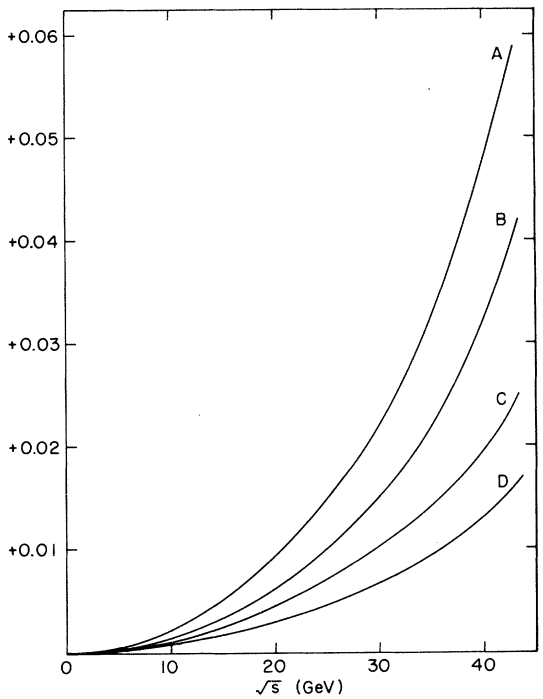

FIG. 2. Forward (H_F) and angular-averaged (H_A) helicities in $e^+e^-\to\mu^+\mu^-$ (in the PEP/PETRA range) in the standard model. A: H_F with $\sin^2\theta_W=0.22$; B: H_F with $\sin^2\theta_W=0.23$; C: H_A with $\sin^2\theta_W=0.22$; D: H_A with $\sin^2\theta_W=0.23$.

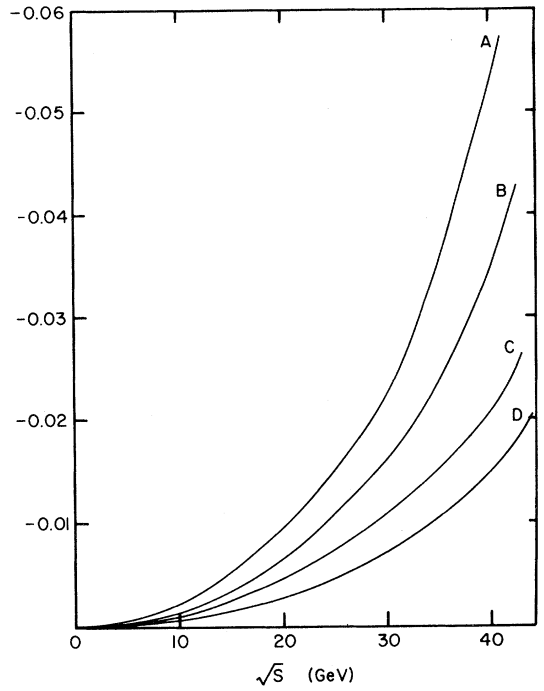

FIG. 3. Same as Fig. 2 but for the LR model. A: H_F ($\sin^2\theta_W=0.28$); B: H_F ($\sin^2\theta_W=0.27$); C: H_A ($\sin^2\theta_W=0.28$); D: H_A ($\sin^2\theta_W=0.27$).

same curves for the LR model in the same energy range. Although the curves are strikingly similar note the difference in the *sign* of the helicities in the two cases. This results from the fact that the magnitude of the vector coupling constant is roughly the same in both models while its sign is *opposite* in the two cases; one sees directly from Eqs. (2.11) and (2.12) that both Σ_1^μ and Σ_2^μ change sign if $v_e\to -v_e$ with a_e left unchanged. Although they differ in sign the magnitude in each case for $\sqrt{s}\lesssim 45$ GeV is too small to measure with the present luminosity. In the future, however, if the sign of the helicity could be measured we would have a clear distinction between the two models. At the present or in the near future, however, it seems unlikely that PEP or PETRA will be able to distinguish the two models.

We now turn to e^+e^- collisions at higher energies such as those to be probed by LEP and the SLAC collider. Apart from the obvious measurement of Z^0 (or $Z^0_{1,2}$) production we look to see what the differences are in the two models off resonance. Figure 4 shows $A_{\rm FB}$ in the energy range above $\sqrt{s}\simeq 45$ GeV for both models; we see immediately that even at $\sqrt{s}\simeq 70$ GeV the two models are easily (10–20% level) distinguishable. Near the (first) Z^0 resonance we see that $A_{\rm FB}$ undergoes a rapid change in sign. This is essentially due to the change in sign of the (first) Z^0 propagator and because $A_{\rm FB}$ near the (first) Z^0 mass is proportional to the vector coupling of the electron to the (first) Z^0 squared (and hence numerically small).

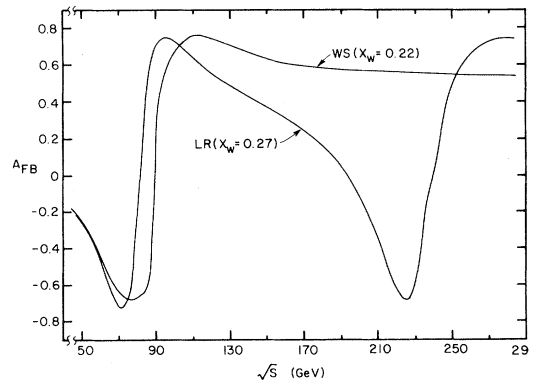

FIG. 4. The forward-backward asymmetry in both models above $\sqrt{s}=45$ GeV for $e^+e^-\to\mu^+\mu^-$.

The behavior of A_{FB} in the two models below $\sqrt{s} \simeq 110-120$ GeV is similar except A_{FB} changes sign earlier in the LR case. Above this region the two models are vastly different, this is mainly due to the rather low ($\simeq 240$ GeV) mass of the second Z^0 in the LR model. While A_{FB} remains roughly flat above $\sqrt{s} \simeq 130$ GeV it again changes sign twice before reaching $\sqrt{s} \simeq M_{Z_2} \simeq 240$ GeV. In this region A_{FB} is controlled by the interference between the contribution of the two Z^0's.

Figure 5 shows the predictions of the two models for the average helicity of the outgoing lepton with $\sqrt{s} \geq 45$ GeV. Note that the helicity remains small in both cases below $\simeq 70-80$ GeV and changes sign in the 80—90 GeV region (again due to the Z^0 propagator sign change). Near the (first) Z^0 resonance the helicity is large, $\sim 30\%$, and can be easily measured, this (apart from the obvious difference in mass) provides a clear test of the LR model in comparison to the WS model. Above the Z^0 resonance region the helicity in the WS model remains roughly flat at $\simeq -0.15$ while in the LR model it remains positive ($\simeq 0.2$) up to $\simeq 200-210$ GeV where it changes sign due to the presence of Z_2 at 240 GeV. A similar set of curves can be drawn for the two models for the forward helicity with similar results.

The analysis presented here seems to show that it is hopeless, either by measuring total cross sections, forward-backward asymmetry, or final-particle helicity to distinguish between the standard model and the LR model at PEP or PETRA energies using unpolarized beams (unless one can at least measure the sign of the helicity of the outgoing lepton). Things are much brighter, however, at higher energies such as those at LEP; apart from the Z^0-mass and branching-ratio measurements we see a large difference in both the forward-backward asymmetry and the average helicity in the two cases. We conclude that a high energy e^+e^- collider can easily test our LR model but it may be impossible to do so at PEP or PETRA.

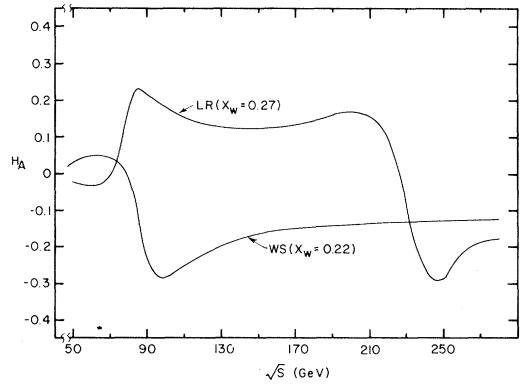

FIG. 5. The average helicity for both models (in $e^+e^- \to \mu^+\mu^-$) above $\sqrt{s} = 45$ GeV.

III. *ep* TESTS

Since the recent experiments on deep-inelastic electron-deuteron scattering at low Q^2 at SLAC[5] it has become increasingly apparent that electron-hadron interactions may be a unique regime for studying the nature of various weak-interaction models. At low Q^2 however, the various neutral-current-produced asymmetries are quite small ($\sim 10^{-5}-10^{-4}$) and extremely difficult to measure. In fact for any reasonable fixed target machine one could not hope to reach Q^2's above $500-700$ GeV^2 with any appreciable cross section. It is just in this region, however, above $Q^2 \simeq 10^3$ GeV^2 that the various asymmetries become more easily measured without all of the complex techniques employed by the SLAC-Yale group.

In *ep* collisions with unpolarized protons we can imagine four possible neutral-current cross sections, one for each helicity and charge of the initial *e*:

$$\sigma(e^{\pm}_{L,R}) \,. \tag{3.1}$$

With these cross sections we can construct various asymmetries produced by parity- and charge-conjugation-violating neutral-gauge-boson exchange(s) interfering with the photon-exchange term. Consider the subprocess $e^- q^i_{L(R)} \to e^- q^i_{L(R)}$ where $q^i_{L(R)}$ is a left- (right-) handed quark of type *i*. If we denote the coupling of the electrons and quarks to the photon and Z bosons by[6] (α labels the Z bosons)

$$\mathcal{L} = \bar{f}[\tfrac{1}{2}\gamma_\mu(1+\gamma_5)Q^{\gamma,Z^\alpha}_{Lf} + \tfrac{1}{2}\gamma_\mu(1-\gamma_5)Q^{\gamma,Z^\alpha}_{Rf}]f \times \begin{Bmatrix} A^\mu \\ Z^\mu_\alpha \end{Bmatrix} \tag{3.2}$$

with the obvious requirement $Q^\gamma_{Lf} = Q^\gamma_{Rf} = Q^\gamma_f$ we can obtain the following cross sections:

$$d\sigma^i_{RR} \propto \left| \frac{Q^\gamma_{Re} Q^\gamma_{Ri}}{Q^2} + \sum_\alpha \frac{Q^{Z^\alpha}_{Re} Q^{Z^\alpha}_{Ri}}{Q^2 + M_{Z_\alpha}{}^2} \right|^2, \quad d\sigma^i_{RL} \propto \left| \frac{Q^\gamma_{Re} Q^\gamma_{Li}}{Q^2} + \sum_\alpha \frac{Q^{Z^\alpha}_{Re} Q^{Z^\alpha}_{Li}}{Q^2 + M_{Z_\alpha}{}^2} \right|^2 (1-y)^2 ,$$
$$d\sigma^i_{LL} \propto \left| \frac{Q^\gamma_{Le} Q^\gamma_{Li}}{Q^2} + \sum_\alpha \frac{Q^{Z^\alpha}_{Le} Q^{Z^\alpha}_{Li}}{Q^2 + M^2_{Z_\alpha}} \right|^2, \quad d\sigma^i_{LR} \propto \left| \frac{Q^\gamma_{Le} Q^\gamma_{Ri}}{Q^2} + \sum_\alpha \frac{Q^{Z^\alpha}_{Le} Q^{Z^\alpha}_{Ri}}{Q^2 + M_{Z_\alpha}{}^2} \right|^2 (1-y)^2 , \tag{3.3}$$

where $d\sigma^i_{L(R)L(R)}$ represents the differential cross section for scattering left- (right-) handed electrons on left- (right-) handed quarks of type i. For antiparticles the left- and right-handed couplings are interchanged and the sign is reversed, e.g.,

$$Q_L(e^+) = -Q_R(e^-) ,$$
$$Q_R(e^+) = -Q_L(e^-) . \tag{3.4}$$

This ensures that the vector coupling constant of the antiparticle is opposite in sign to that of the corresponding particle while the axial coupling constant remains unchanged. The variable y is the usual scaling variable of deep-inelastic scattering.

The total contribution to the above cross sections is obtained by multiplying each $d\sigma^i$ by the corresponding weight factor (the quark distribution function in the target hadron) and summing over quarks and antiquarks. We find

$$d\sigma(e^-_R) = \sum_i (d\sigma^i_{RL} + d\sigma^i_{RR}) x q_i(x) ,$$
$$d\sigma(e^-_L) = \sum_i (d\sigma^i_{LL} + d\sigma^i_{LR}) x q_i(x) \tag{3.5}$$

with $xq_i(x)$ being the quark (and antiquark) distribution functions for the target hadron. Within the standard model we have only a angle Z^0 with

$$Q^Z_{Li} = \frac{e(T^i_{3L} - x_W Q^\gamma_i)}{[x_W(1-x_W)]^{1/2}} ,$$
$$Q^Z_{Ri} = \frac{-e x_W Q^\gamma_i}{[x_W(1-x_W)]^{1/2}} . \tag{3.6}$$

Similar expressions can be written down for positrons. Once the $xq_i(x)$ are known we can immediately calculate the various cross sections which will be functions of x and y in general. Since these are doubly differential (too differential for our purposes) we will integrate over all x and examine $d\sigma/dy$ only. We will make use of the Q^2-dependent distribution functions of Buras and Gaemers[7] in order to include lowest-order QCD scaling violations in our calculation. These corrections are, however, quite insignificant at these Q^2 values as shown in our earlier work.[2]

We now turn to the various possible asymmetry parameters we will examine below; we define

$$A^\pm(y) = \frac{\frac{d\sigma}{dy}(e^\pm_R) - \frac{d\sigma}{dy}(e^\pm_L)}{\frac{d\sigma}{dy}(e^\pm_R) + \frac{d\sigma}{dy}(e^\pm_L)} , \tag{3.7}$$

$$B^\pm(y) = \frac{\frac{d\sigma}{dy}(e^\pm_R) - \frac{d\sigma}{dy}(e^\mp_L)}{\frac{d\sigma}{dy}(e^\pm_R) + \frac{d\sigma}{dy}(e^\mp_L)} , \tag{3.8}$$

$$C_{L,R}(y) = \frac{\frac{d\sigma}{dy}(e^+_{L,R}) - \frac{d\sigma}{dy}(e^-_{L,R})}{\frac{d\sigma}{dy}(e^+_{L,R}) + \frac{d\sigma}{dy}(e^-_{L,R})} . \tag{3.9}$$

Note that these six asymmetries are clearly not all independent since there are only four measurable cross sections $d\sigma(e^\pm_{L,R})/dy$. For low Q^2 all of these cross sections rise like Q^2 such that, say, A^-/Q^2 is essentially independent of Q^2 until Q^2's near gauge-boson masses are reached. The typical behavior of these asymmetries with Q^2 can be seen in Fig. 6. In the low-Q^2 region ($Q^2 \lesssim 10^2$ GeV$^2/c^2$), A^-/Q^2 is essentially flat with a value typical of the SLAC-Yale experiment. (We fix $y=0.2$ and take the standard model for simplicity. The same qualitative results are obtained for different y values as well as for the LR model.) The Q^2 dependence for larger Q^2 values comes from both the Q^2 dependence of the Z^0-boson propagator as well as the Q^2-dependent distribution functions; the last of these is actually a small effect in the *ratios* of cross sections like (3.7)–(3.9). Although A^-/Q^2 *decreases* with increasing Q^2, the actual asymmetry A^- rises quite rapidly. For example, at $Q^2 \simeq 10^4$ GeV we see that $A^- \simeq 0.25$, several orders of magnitude larger than the value obtained by the SLAC-Yale group. Certainly, asymmetries of such an order of magnitude are easily measurable with good statistics and the advantages of high-Q^2 ep interactions are clearly seen. Above $Q^2 \simeq 10^4$ GeV$^2/c^2$ or so the rapid

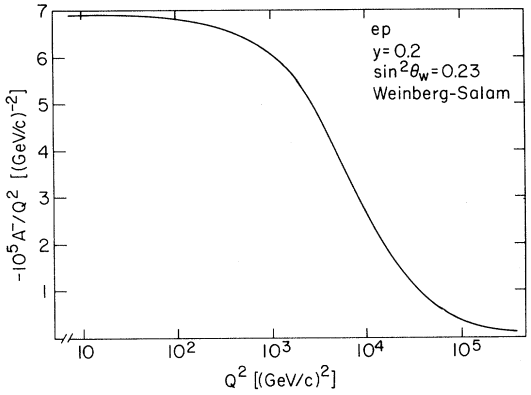

FIG. 6. A^-/Q^2 as a function of Q^2 in the standard model for *ep* deep-inelastic scattering with $y=0.2$.

growth in the various asymmetries levels off until they reach constant values in the asymptotic region $Q^2 >>$ all gauge-boson masses. The asymptotic region for the standard model can already be achieved (?) by the HERA design ($Q^2 \simeq 10^5$ GeV$^2/c^2$) while, for the LR model, it is outside the reach of any proposed machine ($\gtrsim 6\times 10^5$ GeV$^2/c^2$).

We now turn to a comparison of the predictions of the WS and LR models for the various asymmetries, we will take $Q^2=10^4$ GeV$^2/c^2$ since, certainly, this is a value that all the proposed *ep* machines can easily reach. Figure 7(a) shows a plot of $A^+(y)$ with $Q^2=10^4$ GeV$^2/c^2$ for both the WS and LR models while Fig. 7(b) shows $A^-(y)$ for the same Q^2 for the same two models. We see that in both of these cases the two models are clearly distinguishable with different magnitudes as well as different y dependences. [Note that $A^{\pm}(y)$ is a true measure of parity-violating neutral-current effects while, for example, $C_{L,R}$ measure charge-conjugation-violating interactions. $B^{\pm}$ measure simultaneous parity and charge-conjugation violations.] Figure 8 shows the plots for B^- and $-B^+$ for both the LR and WS models at $Q^2=10^4$ GeV$^2/c^2$. Note that unlike the $A^{\pm}$ case the curves are quite similar and, even at large y, would require measurements at better than the 5% level in order to distinguish between the two models. Figures 9 and 10 show C_L and C_R, respectively, for the same two models at the same Q^2. Here, unlike the curves in Fig. 8, we again see a clear distinction in the predictions for the magnitudes for the two models although their y dependences are seen to be quite similar.

It is clear here that measurements of these asymmetries at $Q^2 \simeq 10^4$ GeV$^2/c^2$ for various values of y can be used to easily distinguish between the standard and LR models.

These two models not only differ in their neutral-current sector but also in the charged-current sector. Whereas the cross section for the charged-current reaction

$$e_R^- p \rightarrow \nu_R(?)X \tag{3.10}$$

is zero in the standard model (since ν_R, if it exists, does not couple to W^-) a reaction of this sort is

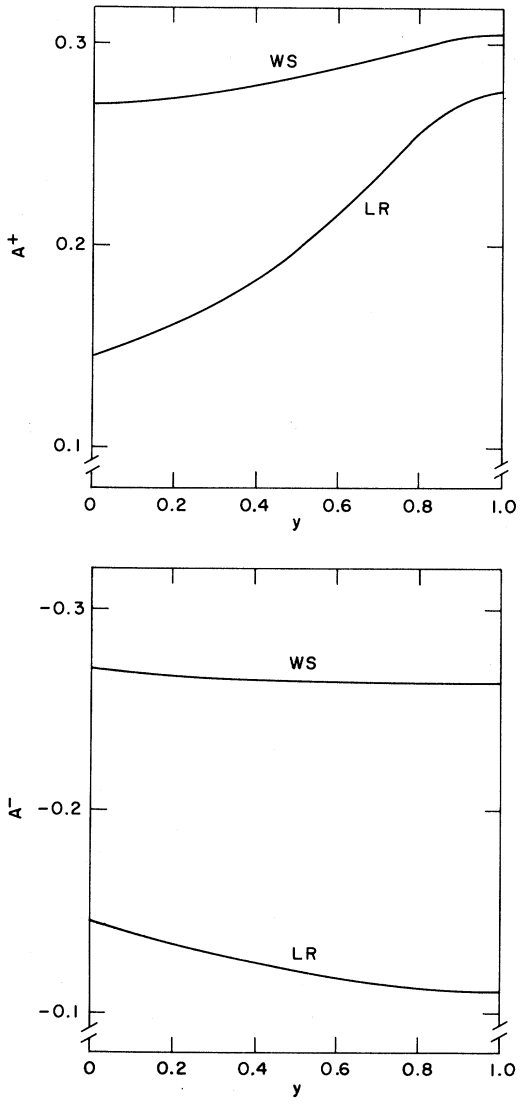

FIG. 7. (a) $A^+(y)$ in both models at $Q^2=10^4$ GeV$^2/c^2$. (b) $A^-(y)$ at the same Q^2.

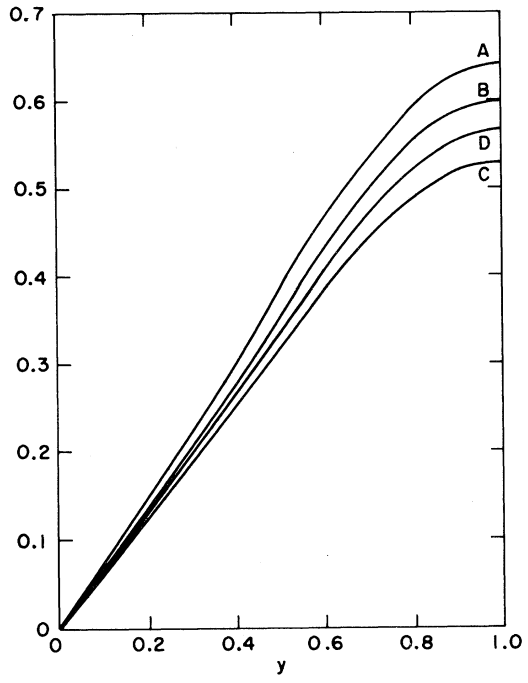

FIG. 8. $B^{\pm}(y)$ at $Q^2=10^4$ GeV$^2/c^2$ for both models. A: $B^-(y)$ in the LR model with $\sin^2\theta_W=0.27$; B: $B^-(y)$ in the WS model with $\sin^2\theta_W=0.23$; C: $-B^+(y)$ for the LR model with $\sin^2\theta_W=0.27$; D: $-B^+(y)$ for the WS model with $\sin^2\theta_W=0.23$.

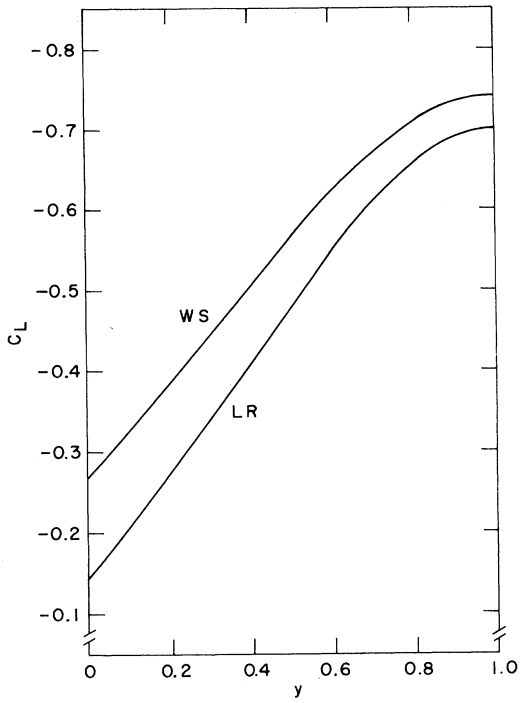

FIG. 9. $C_L(y)$ for both models at $Q^2=10^4$ GeV$^2/c^2$.

possible in the LR model:

$$e_R^- p \to NX \ , \tag{3.10'}$$

where N is a heavy ($\sim$10's of GeV) right-handed Majorana neutrino. This reaction has already been discussed,[8] however, so we will not discuss it further here but say only that it also provides a clear test of the LR model.

One thing should be stressed at this point. In order to do weak-interaction tests in high-Q^2 ep machines it is necessary to have polarized beams and to be able to accelerate both electrons and positrons. All future proposed ep machines have made provisions for these possibilities in their design.

In summary we see that the ep physics provides a unique[9] area for studying neutral- and charged-current processes which can be used to test electroweak models in ways clearly different from e^+e^- or $\overset{(-)}{p}\,p$ colliders.

IV. DISCUSSION AND CONCLUSIONS

As we have seen future e^+e^- and ep collider facilities may provide a proving ground for the standard electroweak theory $SU(2)_L \otimes U(1)$ and the alternative $SU(2)_L \otimes SU(2)_R \otimes U(1)_{B-L}$ left-right-symmetric theory considered here. At rather low Q^2 (i.e., present experiments) the two models are completely identical except for differences at the level of a few percent. The only exception to this is the sign of the helicity of the out-going lepton in e^+e^- experiments in the PEP/PETRA energy range; however, it seems that a measurement of this quantity at the level necessary to test the two models presented here is impossible at present (or in the very near future). What we need is some way to measure accurately the magnitude *and* sign of the electron neutral-current coupling constant—this is made difficult by the fact that $\sin^2\theta_W \simeq \frac{1}{4}$ in both models where this coupling essentially vanishes.

Apart from the direct observation of the (first) Z^0 boson by LEP or the SLAC collider, we have seen that measurements of the forward-backward asymmetry and the out-going helicity for the process $e^+e^- \to \mu^+\mu^-$ (or $\tau^+\tau^-$) can easily provide a clear distinction between the two models investigat-

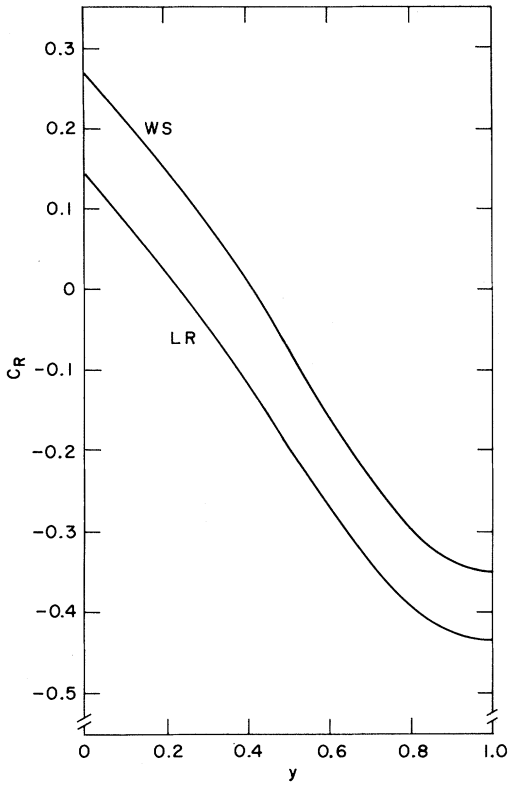

FIG. 10. $C_R(y)$ for both models at $Q^2=10^4$ GeV$^2/c^2$.

ed here. The only requirement is either very accurate measurements at $\sqrt{s}\simeq 30-40$ GeV or somewhat more coarse measurements at or near $\sqrt{s}\simeq 70$ GeV where A_{FB} is quite large ($\simeq -0.7$). Certainly these energies are obtainable in the planned colliders of this kind. Helicities, on the other hand, do not get appreciably large until $\sqrt{s}\simeq 70$ GeV/c; however, to distinguish the two models under consideration we need only measure the *sign* of the helicity which may be easier than an actual magnitude measurement.

We have found that *ep* colliders, if they have polarized beams and can accelerate both e^+ and e^-, provide a unique opportunity to examine the various lepton and quark couplings. One might imagine, perhaps, the following scenario: It is found that the Z^0 boson is lighter than expected which usually implies that the true model has (at least) two Z^0 bosons. By sitting on this Z^0, we could then extract its various couplings to quarks and leptons but we are unable to produce the heavier Z^0 (Z_2^0) due to its large mass and extract similar coupling constants. We could, however, extract at least some of this information from the various *ep* asymmetries if we feed in what we have learned from sitting on the Z_1^0. This new information would not be obtained if we used e^+e^- or $\overset{(-)}{p}p$ colliders alone with insufficient $\sqrt{s}$ to produce the second Z^0. The *ep* machine with its ZP exchange in the t channel would, however, give us some idea of properties of the second Z^0. Given the mass of Z_2^0 ($\simeq 240$ GeV) this seems a likely prospect if the LR model is correct and present plans for the future e^+e^- and $\overset{(-)}{p}p$ colliders go through. (The latter have insufficient $\sqrt{s}$ to produce Z_2^0 at significant rates to extract useful information at least for the first-generation designs.)

Since these high-energy machines are not far off in the future it may not be long before we can test the standard model as well as the possibility of low-energy parity restoration through the alternative left-right-symmetric model.

ACKNOWLEDGMENTS

The author would like to thank G. Senjanović, W. Marciano, and W. Y. Lee for discussions related to this work. This work was supported in part by the U. S. Department of Energy by Iowa State University under Contract No. W-7405-ENG-82. This article was supported by the Director for High Energy Physics, Office of Basic Sciences.

APPENDIX

In this appendix we give for the sake of reference the exact expressions for the various weak asymmetries at low Q^2 in the standard model:

$$A^{\pm}(x,y)=\frac{G_F Q^2}{\sqrt{2}\pi\alpha}\frac{\sum_i Q_i[xq_i(x)]}{\left(\sum_i Q_i^2[xq_i(x)]\right.}[\pm g_A^e g_V^i + g_V^e g_A^i F(y)]\ . \tag{A1}$$

$g_{V(A)}^e$ is the electron vector (axial-vector) coupling constant and $g_{V(A)}^i$ is the vector (axial-vector) coupling constant for the ith quark of charge Q_i and with distribution function $xq_i(x)$:

$$F(y)\equiv\frac{1-(1-y)^2}{1+(1-y)^2}\ . \tag{A2}$$

In the valence-quark limit we take the approximation that $xu(x)=2xd(x)$ and neglect all sea quarks in the proton for all Q^2. In this approximation we find

$$A_v^{\pm}(y)=\frac{G_F Q^2}{2\sqrt{2}\pi\alpha}[\pm(\tfrac{5}{6}-2x_W)-(1-4x_W)F(y)]\ . \tag{A3}$$

Similarly we find

$$B^{\pm}(x,y)=\frac{G_F Q^2}{\sqrt{2}\pi\alpha}\frac{\sum_i Q_i[xq_i(x)]}{\sum_i Q_i^2[xq_i(x)]}F(y)g_A^i(g_V^e\pm g_A^e) \tag{A4}$$

which in the valence limit gives

$$B_v(y)=\frac{5}{12}\frac{G_F Q^2}{\sqrt{2}\pi\alpha}F(y)[\pm 1+(1-4x_W)] \tag{A5}$$

and

$$C_{L,R}(x,y)=\frac{G_F Q^2}{\sqrt{2}\pi\alpha}\frac{\sum_i Q_i[xq_i(x)]}{\sum_i Q_i^2[xq_i(x)]}[\pm g_A^e g_V^i+g_A^e g_A^i F(y)] \tag{A6}$$

with the valence limit of

$$[C_{L,R}(y)]_v=\frac{G_F Q^2}{2\sqrt{2}\pi\alpha}[\pm(\tfrac{5}{6}-2x_W)-\tfrac{5}{6}F(y)]\ . \tag{A7}$$

Note that in this low-Q^2 region all of the various asymmetries are linear in Q^2 resulting from the Z^0-boson propagator. We also note that the valence-quark approximation is a rather good one for the ratios of cross sections like the asymmetries above.

---

[1]T. G. Rizzo and G. Senjanović, Phys. Rev. Lett. 46, 1315 (1981); Phys. Rev. D 24, 704 (1981); and Brookhaven Report Nos. BNL-29796 and BNL-29716, 1981 (unpublished).

[2]For a review of SU(5) and grand unification in general see P. Langacker, Phys. Rep. 72, 185 (1981).

[3]See, for example, T. G. Rizzo, Phys. Rev. D 20, 2207 (1979); 21, 1214 (1980); see also T. G. Rizzo and D. P. Sidhu, Phys. Rev. *ibid.* 21, 1209 (1980).

[4]To see how this is done see M. J. Puhala, Z. J. Rek, B.-L. Young, and X-T Zhu, Phys. Rev. D 25, 95 (1982).

[5]C. Y. Prescott *et al.*, Phys. Lett. 77B, 347 (1978); 84B, 524 (1979).

[6]We follow the notation of R. N. Cahn and F. J. Gilman, Phys. Rev. D 17, 1313 (1978).

[7]A. J. Buras and K. J. K. Gaemers, Nucl. Phys. B132, 249 (1978).

[8]See the last paper of Ref. 1 for details of this reaction.

[9]See T. G. Rizzo, in Proceedings of the 1981 ISABELLE Summer Study, Brookhaven National Laboratory (unpublished).